Analytical relations for long-droplet breakup in asymmetric T junctions

Ahmad Bedram, Ali Moosavi,* and Siamak Kazemzadeh Hannani
Center of Excellence in Energy Conversion (CEEC), School of Mechanical Engineering, Sharif University of Technology, Azadi Avenue, P. O. Box 11365–9567, Tehran, Iran
(Received 4 January 2015; published 18 May 2015)

We develop accurate analytical relations for the droplet volume ratio, droplet length during breakup process, and pressure drop of asymmetric T junctions with a valve in each of the branches for producing unequal-sized droplets. An important advantage of this system is that after manufacturing the system, the size of the generated droplets can be changed simply by adjusting the valves. The results indicate that if the valve ratio is smaller than 0.65, the system enters a nonbreakup regime. Also the pressure drop does not depend on the time and decreases by increasing the valve ratio, namely, opening the degree of valve 1 to valve 2. In addition, the results reveal that by decreasing (increasing) the valve ratio, the droplet length of branch 1 decreases (increases) and the droplet length of branch 2 increases (decreases) linearly while the whole length of the droplet remains unchanged.

DOI: 10.1103/PhysRevE.91.053012 PACS number(s): 47.61.−k, 47.55.df, 68.05.Cf, 47.11.Df

I. INTRODUCTION

Improving the performance of droplet-based microfluidics is a prerequisite for optimizing many procedures such as biological and chemical reactions, material synthesis, and DNA analysis. Microdroplets act as excellent microreactors that improve the heat and mass transfer due to high mixing inside the droplet [1,2]. Droplet-based microfluidics contain various droplet processes such as transport [3], symmetric breakup [4,5], asymmetric breakup [6,7], merging [8], generation [9,10], and storage [11]. The processes that use microdroplets have many advantages such as monitoring the kinetic of the process by means of the droplet motion, generating the samples with precise volume and production rate, and no dispersion of droplet in the base fluid [12–14].

For increasing the production rate of the droplets, various methods are available including dividing an initial droplet into a large number of small droplets by means of geometrical facilities such as symmetric T junctions [4,5,15–17]. However, a symmetric breakup process cannot be used for the production of unequal-sized droplets which are used in many applications such as the chemical and pharmaceutical industries. Moreover, the symmetric breakup process has only one, nonarbitrary production rate. In order to resolve such problems, a number of methods has been proposed. One of the methods for producing unequal-sized droplets relies on using an obstacle in the channels [18]. The disadvantage of this method is that the small and large droplets after the obstacle are moving together and another process is needed to separate them. A different method is based on using a T junction with unequal length branches [18]. This method increases the pressure drop and the manufacturing costs for small volume ratios, namely, the volume ratio of the small droplet to the large droplet after breakup. A T junction with unequal width branches is a method that does not have the disadvantage of T junctions with unequal length branches [19]. However, after manufacturing the system, only a specific volume ratio can be generated. There is a method without any T junction in which the droplets move through a vertical tube and break up into unequal smaller droplets for Weber numbers less than 5 [20]. The disadvantage of this method is that after breakup of the initial droplets, the small generated droplets are moving together. A different suggested method is based on using a pneumatic valve inside of a tube such that the consecutive droplets break up into smaller ones by transferring through the pneumatic valve [21]. The pressure of the pneumatic valve determines the volume ratio of the generated droplets. The disadvantage of this method is that the size of the generated droplets is not controllable precisely because of affecting the pressure of the flow on the valve performance. There is a heat-transfer-based method in which a heater has been placed in one of the branches of the symmetric T junction [22]. By heating the fluid of the branch, the viscosity and hydrodynamic resistance of the fluid reduce and the larger droplet enters into it. The disadvantage of this method is that for producing a small volume ratio, the heater temperature should be high and it is possible that the nature of the continuity or the droplet changes. Also the fluids may be vaporized, especially in the locations with low pressure. For example, in Ref. [22], it has been stated that for high capillary numbers, the temperature should reach 40 °C for generating the appropriate volume ratios, which is not acceptable especially for biologic applications. There are some other methods for breaking an initial droplet into unequal-sized droplets such as droplet breakup in the turbulent flow [23–25], using a cylinder inside a tube that the droplet is transferred through [26], passing the droplet from microfluidic cross flows [27], droplet breakup in a simple shear flow [28–31], arrival of two droplets to a main branch of a symmetric T junction with a small time difference [32], T junctions with unequal length branches [33–35], using two convergent-divergent consecutive symmetric T junctions [36], droplet motion in a domain with gravity or body force [37–39], and heat-transfer-based methods [40]. These methods have disadvantages similar to those already mentioned.

In this study, we consider a two-dimensional (2D) T junction with one valve in each of the branches for producing unequal-sized droplets [41]. The valves are, in fact, adjustable orifice plates and, after manufacturing the system, one can

*Corresponding author: moosavi@sharif.edu

adjust the opening degree of the orifices. Therefore, the adjustable orifice can act as a valve because it can tune the opening degree of the channel up to an arbitrary amount. So we refer to the adjustable orifice plate as a valve. The application and structure of the adjustable orifice valves are investigated in various research papers [42–44]. This method does not have the disadvantages of the other available methods and, after manufacturing the system, one can adjust the volume ratio simply. For investigating the droplet breakup process, an analytical theory and numerical simulation, based on a volume of fluid (VOF) algorithm, are used. The results of the simulations were verified using two benchmarks [45,46] and very good agreement was observed. Numerical simulation is conducted for validating the analytical results and very good agreement has been found between the results. In the analytical theory, first we calculate the pressure drop of the continuous fluid through the valves. Afterward, we use this relation to derive a relation for the calculation of the volume ratio of the generated droplets after breakup. Then we obtain accurate relations for droplet length and pressure drop of the system. These relations have very good agreement with our numerical results. We show that when the droplet is deforming in the center of the junction, the length growth rate of the droplet that enters the branch with the more open valve is more than that of the droplet that enters the other branch. Also we show that the pressure drop of the system is independent of time and reduces with increase of the valve ratio, as by increasing the valve ratio the system approaches to the geometry of a symmetric T junction.

In the subject of droplet motion in 3D rectangular cross-section channels, the results of the 2D solution are not representative of the 3D solution due to the presence of the gutter regions in the corners of the channel cross section. The gutter regions affect the pressure drop of the system [47]. But for the case of the T junction with the valve, the main sources of the pressure drop are valves and straight tubes. Therefore, the effect of the gutter region becomes small and the 2D results can qualitatively represent the 3D solution [41]. Therefore, we expect that our results will carry over qualitatively to the behavior of 3D systems.

II. THE SYSTEM GEOMETRY

Figure 1 illustrates the geometry of the considered system. When a long droplet passes through this system, it breaks up into unequal parts. There is a valve in each of the branches and the opening degree of the valves adjusts the volume ratio of the generated droplets. Droplet length is long enough to fill the entire branch and z_1 and z_2 do not vanish until the end of the process. The distance between the valves and the system outlets is equal to $3w$, where w is the channel width.

We define some parameters of the problem. *Valve ratio* is the ratio of the opening degree of valve 1 to valve 2 ($\lambda = s_1/s_2$). *Volume ratio* is the ratio of the smaller droplet to the larger droplet after breakup ($\tau = V_1/V_2$). The capillary number is defined as $\mathrm{Ca} = \mu_c U_{\mathrm{in}}/\sigma$, with μ_c as the dynamic viscosity of continuous fluid, U_{in} as the fluid velocity in the inlet of the system, and σ as the surface tension between two fluids. The capillary number represents the ratio of the inertial forces to the surface tension forces. The width of the inlet channel and branches (w) is supposed to be equal to 20×10^{-6}m. L_{initial} is the droplet length when it is in the inlet channel that is $6w$. L_{in} is the length of the inlet channel that is equal to $9w$. The capillary number is supposed to be 0.01. L is the branch length that is $15.5w$.

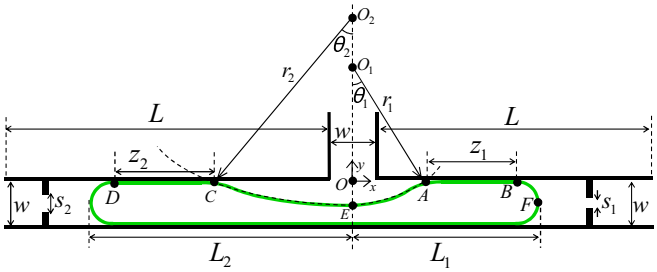

FIG. 1. (Color online) A schematic representation of the system with the related parameters. The droplet tips (for example, point F) do not reach the valves until the end of the breakup process. Subscriptions 1 and 2 represent right and left branches, respectively. z is the contact length between the upper surface of the droplet and the wall. L and w are the length and width of the branches, respectively. r and O are the radius and center of the curvature of the droplet upper surface, respectively. s is the opening degree of the valve. θ_1 represents the angle between the y axis and the line O_1A where the points A and B are the first and the end points of the contact line between the upper surface of the droplet and the wall (θ_2 is similar). L_1 and L_2 are the droplet lengths. Points F and E are the droplet tip and intersection of the y axis and the droplet upper surface, respectively.

III. ANALYTICAL THEORY

A. Transformation of coordinate system

In this section, we present an analytical theory for investigating the long-droplet breakup in a T junction with a valve. The valve of the T junction may be considered as a plate with a gap within it (Fig. 1). For the analytical investigation of long-droplet breakup, we should first calculate the pressure drop of the continuous fluid through the valves. For this purpose, we use new coordinates χ and ξ (elliptic cylindrical coordinates) and calculate the pressure drop through a venturi, as depicted in Fig. 3. Finally, we set the curvature radius of the venturi walls to zero to obtain a relation for the pressure drop through a plate with a gap. Then we use this relation and calculate the volume ratio of the generated droplets after breakup. Finally, using the relations for the pressure drop and volume ratio, we derive relations for determining the droplet length and pressure drop of the system.

We want to calculate the pressure drop of fluid through the venturi tube. For this purpose, first we define new coordinates χ and ξ as follows:

$$x = c\,\cosh\xi\,\cos\chi, \quad y = c\,\sinh\xi\,\sin\chi, \tag{1}$$

where c is a constant. For constant values of ξ from Eq. (1), we have

$$\frac{y^2}{c^2\sinh^2\xi} + \frac{x^2}{c^2\cosh^2\xi} = 1. \tag{2}$$

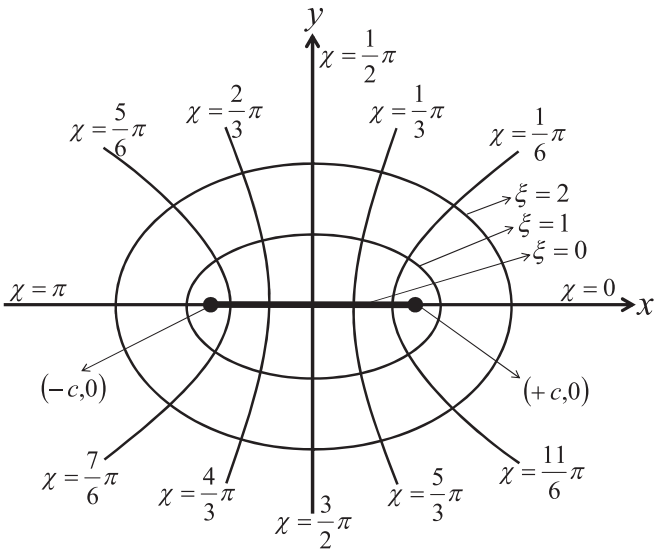

FIG. 2. χ and ξ coordinates relative to x and y coordinates.

Therefore, $\xi = \text{const}$ curves are concentric ellipses, as depicted in Fig. 2. Similarly, it can be shown that $\chi = \text{const}$ curves are confocal hyperbolas.

As can be concluded from Fig. 2, the range of variables is $0 \leqslant \chi < 2\pi$ and $0 \leqslant \xi < \infty$. For investigating the flow in a venturi, it is assumed that we have a tube with the walls as $\chi = \text{const}$ lines. Now, in order to remove the trigonometric and hyperbolic functions in the subsequent expressions, we apply the following change of variables:

$$\varpi = \cosh\xi\,, \quad \zeta = \cos\chi\,. \tag{3}$$

By substituting Eq. (3) in Eq. (1), we have

$$x = c\varpi\zeta, \quad y = c\sqrt{\varpi^2 - 1}\sqrt{1-\zeta^2}. \tag{4}$$

Through using these variables, $\zeta = \text{const}$ lines are confocal hyperbolas and $\varpi = \text{const}$ lines are concentric ellipses. Therefore, the geometry of our problem (venturi) becomes as depicted in Fig. 3.

B. Deriving the pressure drop through the valve

The flow in the venturi is incompressible, laminar, and steady state. Therefore, the governing equations of the problem are Navier-Stokes and continuity as follows:

$$\mu\nabla^2\vec{V} = \vec{\nabla}P, \quad \vec{\nabla}\cdot\vec{V} = 0. \tag{5}$$

Using the vectors' properties, one has [48]

$$\nabla^2\vec{V} = \vec{\nabla}(\vec{\nabla}\cdot\vec{V}) - \vec{\nabla}\times(\vec{\nabla}\times\vec{V}), \tag{6}$$

where the term $\vec{\nabla}\cdot\vec{V}$ is zero (according to continuity). By substituting Eq. (6) to Eq. (5) and taking a curl from both sides of it, we have (note that the curl of term $\vec{\nabla}\times\vec{\nabla}P$ is zero)

$$\vec{\nabla}\times[\vec{\nabla}\times(\vec{\nabla}\times\vec{V})] = 0. \tag{7}$$

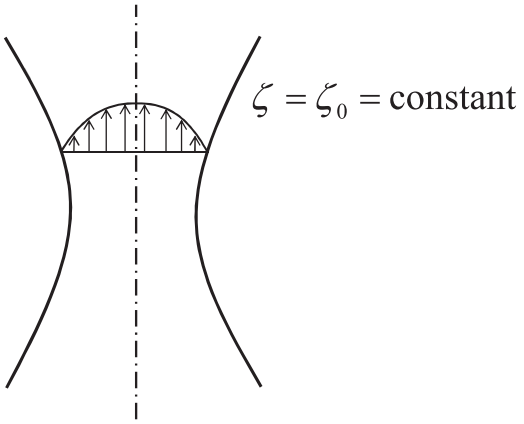

FIG. 3. Flow in the venturi tube. The walls are $\zeta = \text{const}$ lines.

Equation (7) and the continuity are governing equations of the venturi problem (Fig. 3). For converting a Cartesian coordinate to a curvilinear one, the inner and exterior products change according to the tensor notation (Levi-Civita) as follows [49]:

$$\vec{\nabla}\cdot\vec{\Gamma} = H\frac{\partial}{\partial\kappa_k}\left(\frac{h_k}{H}\Gamma_k\right)$$
$$(\vec{\nabla}\times\vec{\Gamma})_k = \frac{H\,\hat{e}_k}{h_k}\varepsilon_{ijk}\frac{\partial}{\partial\kappa_i}\left(\frac{\Gamma_j}{h_j}\right), \tag{8}$$

where $H = h_1h_2h_3$ and $\vec{\Gamma}$ is a vector variable. κ_1, κ_2, and κ_3 are curvilinear coordinate axes. $\hat{e}_1$, $\hat{e}_2$, and $\hat{e}_3$ are unit vectors in the direction of κ_1, κ_2, and κ_3. h_1, h_2, and h_3 are scale factors of the coordinate system that are computed from the following relation [49]:

$$\frac{1}{h_i^2} = \left(\frac{\partial x}{\partial\kappa_i}\right)^2 + \left(\frac{\partial y}{\partial\kappa_i}\right)^2 + \left(\frac{\partial z}{\partial\kappa_i}\right)^2. \tag{9}$$

The value of h_i is calculated using Eqs. (4) and (9). By substituting h_i in Eq. (8), the continuity equation will be represented as

$$\frac{\partial}{\partial\varpi}\left(\frac{c\sqrt{\varpi^2-\zeta^2}}{\sqrt{1-\zeta^2}}V_\varpi\right) + \frac{\partial}{\partial\zeta}\left(\frac{c\sqrt{\varpi^2-\zeta^2}}{\sqrt{\varpi^2-1}}V_\zeta\right) = 0. \tag{10}$$

If we define the stream function as the following relations, the continuity equation [Eq. (10)] is satisfied:

$$V_\varpi = \frac{\sqrt{1-\zeta^2}}{c\sqrt{\varpi^2-\zeta^2}}\frac{\partial\psi}{\partial\zeta}, \quad V_\zeta = -\frac{\sqrt{\varpi^2-1}}{c\sqrt{\varpi^2-\zeta^2}}\frac{\partial\psi}{\partial\varpi}. \tag{11}$$

According to Fig. 3, we assume that the streamlines are confocal hyperbolas. In other words, the streamlines are $\zeta = \text{const}$ lines. Therefore, the stream function depends only on ζ or $\psi = \psi(\zeta)$. Now with three consecutive times using Eq. (8), the Navier-Stokes equation [Eq. (7)] can be

rewritten as

$$\vec{\nabla}\times[\vec{\nabla}\times(\vec{\nabla}\times\vec{V})]=\left[0,0,\frac{1}{c^4(\varpi^2-\zeta^2)^4}\sum_{i=1}^{8}\Lambda_i\right],$$

$$\Lambda_1=[-4\varpi^4+(6-4\zeta^2)\varpi^2+2\zeta^2]\times\left[\zeta\frac{\partial\psi}{\partial\zeta}-(1-\zeta^2)\frac{\partial^2\psi}{\partial\zeta^2}\right],$$

$$\Lambda_2=(\varpi^2-\zeta^2)^2\left[\zeta\frac{\partial\psi}{\partial\zeta}+3\zeta^2\frac{\partial^2\psi}{\partial\zeta^2}-\zeta(1-\zeta^2)\frac{\partial^3\psi}{\partial\zeta^3}\right],$$

$$\Lambda_3=(\varpi^2-\zeta^2)\left[2\zeta^3\frac{\partial\psi}{\partial\zeta}-2\zeta^2(1-\zeta^2)\frac{\partial^2\psi}{\partial\zeta^2}\right],\quad \Lambda_4=\varpi^4(\zeta^2-1)\left[4\frac{\partial^2\psi}{\partial\zeta^2}+5\zeta\frac{\partial^3\psi}{\partial\zeta^3}-(1-\zeta^2)\frac{\partial^4\psi}{\partial\zeta^4}\right],$$

$$\Lambda_5=\varpi^2(\zeta^2-1)\left[(-6\zeta^3-4\zeta)\frac{\partial^3\psi}{\partial\zeta^3}+2\zeta^2(1-\zeta^2)\frac{\partial^4\psi}{\partial\zeta^4}\right],$$

$$\Lambda_6=\varpi^2(\zeta^2-1)\left[6\zeta\frac{\partial\psi}{\partial\zeta}+(6\zeta^2-2)\frac{\partial^2\psi}{\partial\zeta^2}\right],\quad \Lambda_7=(\zeta^2-1)\left[2\zeta^3\frac{\partial\psi}{\partial\zeta}+(-2\zeta^4-6\zeta^2)\frac{\partial^2\psi}{\partial\zeta^2}\right],$$

$$\Lambda_8=(\zeta^2-1)\left[(\zeta^5+4\zeta^3)\frac{\partial^3\psi}{\partial\zeta^3}-\zeta^4(1-\zeta^2)\frac{\partial^4\psi}{\partial\zeta^4}\right]. \tag{12}$$

In order to satisfy the Navier-Stokes equation, we should have $\sum_{i=1}^{8}\Lambda_i=0$. By simplifying Eq. (12), one obtains

$$\sum_{i=1}^{8}\Lambda_i=\varpi^4\Gamma(\zeta)+\varpi^2\Theta(\zeta)+\Omega(\zeta)=0, \tag{13}$$

where $\Gamma(\zeta)$, $\Theta(\zeta)$, and $\Omega(\zeta)$ are functions of ζ and derivatives of the stream function with respect to ζ. We should have $\Gamma(\zeta)=\Theta(\zeta)=\Omega(\zeta)=0$ to satisfy Eq. (13). Through these, three equations are obtained and two of them are independent as follows:

$$\zeta^4(1-\zeta^2)^2\frac{\partial^4\psi}{\partial\zeta^4}+(2\zeta^7+2\zeta^5-4\zeta^3)\frac{\partial^3\psi}{\partial\zeta^3}+(-\zeta^6+4\zeta^2)\frac{\partial^2\psi}{\partial\zeta^2}+\zeta^5\frac{\partial\psi}{\partial\zeta}=0, \tag{14}$$

$$\zeta^4(1-\zeta^2)^2\frac{\partial^4\psi}{\partial\zeta^4}+(4\zeta^7-2\zeta^5-2\zeta^3)\frac{\partial^3\psi}{\partial\zeta^3}+(\zeta^6+2\zeta^2)\frac{\partial^2\psi}{\partial\zeta^2}-\zeta^5\frac{\partial\psi}{\partial\zeta}=0. \tag{15}$$

By subtracting Eq. (15) from Eq. (14), we have

$$\zeta^3\frac{\partial\psi}{\partial\zeta}+(-\zeta^4+1)\frac{\partial^2\psi}{\partial\zeta^2}+(-\zeta^5+2\zeta^3-\zeta)\frac{\partial^3\psi}{\partial\zeta^3}=0. \tag{16}$$

For solving Eq. (16) and finding $\psi(\zeta)$, three boundary conditions are required. The velocity on the wall is zero. Therefore, from Eq. (11), we have

$$\frac{\partial\psi}{\partial\zeta}=0\quad\text{for}\quad\zeta=\zeta_0, \tag{17}$$

where $\zeta=\zeta_0$ corresponds to the tube wall. The selection of streamline with zero value is arbitrary [50]. Thus, the streamline that corresponds to the tube axis is supposed to be zero. The tube axis corresponds to $\chi=\pi/2$ and, as a result, to $\zeta=0$. Therefore, we have

$$\psi=0\quad\text{for}\quad\zeta=0. \tag{18}$$

The difference between the two streamlines is equal to the volumetric flow rate between them. Therefore, the difference of the values of the right wall streamline and the tube axis streamline is equal to the half of the tube volumetric flow rate (note that the venturi tube is symmetric). Thus, we get

$$\psi(\zeta_0)-\psi(0)=\frac{q}{2}\xrightarrow{\psi(0)=0}\psi(\zeta_0)=\frac{q}{2}. \tag{19}$$

In Fig. 2, for $0<\chi<\pi/2$, we have venturies with various curvatures. If we consider $\chi=0$ and $\chi=\pi$, the venturi tube is converted to a plate with a gap in it. According to Eq. (3), $\chi=0$ and $\chi=\pi$ correspond to $\zeta=1$ and $\zeta=-1$, respectively. Therefore, if in the boundary conditions [Eq. (17) to Eq. (19)] we consider $\zeta_0=\pm1$, the tube venturi problem converts to the problem of flow moving through a plate with a gap in it.

Now, we should calculate the width of the gap. As already stated, $0\leqslant\xi<\infty$. According to Eq. (3), we have $1\leqslant\varpi<\infty$. By substituting $\zeta_0=\pm1$ to Eq. (4), we have $y=0$, $x\leqslant-c$, and $x\geqslant c$. Therefore, the gap width is equal to $2c$. According to Eq. (5), we have $\mu\nabla^2\vec{V}=\vec{\nabla}P$. On the other hand, $\nabla^2\vec{V}=(\nabla^2V_\varpi,\nabla^2V_\zeta)$ and $\vec{\nabla}P=(h_\varpi\frac{\partial P}{\partial\varpi},h_\zeta\frac{\partial P}{\partial\zeta})$. Thus, by substituting V_ϖ and V_ζ from Eq. (11) to Eq. (5), one can obtain

$$\mu\nabla^2\left(\frac{\sqrt{1-\zeta^2}}{c\sqrt{\varpi^2-\zeta^2}}\frac{\partial\psi}{\partial\zeta}\right)=h_\varpi\frac{\partial P}{\partial\varpi}, \tag{20}$$

$$\mu\nabla^2\left(-\frac{\sqrt{\varpi^2-1}}{c\sqrt{\varpi^2-\zeta^2}}\frac{\partial\psi}{\partial\varpi}\right)=h_\zeta\frac{\partial P}{\partial\zeta}. \tag{21}$$

The stream function (ψ) depends only on ζ. Therefore, Eq. (21) is reduced to $\partial P/\partial\zeta=0$. In converting the coordinate system, the Laplace operator according to the tensor notation

[49] is given as

$$\nabla^2\phi = H\frac{\partial}{\partial\kappa_k}\left(\frac{h_k^2}{H}\frac{\partial\varphi}{\partial\kappa_k}\right), \tag{22}$$

where ϕ is a scalar variable. Using Eq. (22) in Eq. (20) and some calculations and simplifications, we obtain

$$\frac{\partial P}{\partial\varpi} = \frac{\mu}{c^2}\frac{-(\varpi^2+2\zeta^2)\sqrt{\varpi^2-1}+(\varpi^2+\zeta^2)\sqrt{1-\zeta^2}}{(\varpi^2-\zeta^2)^{2.5}}\frac{\partial\psi}{\partial\zeta} + \frac{\mu}{c^2}\frac{-3\zeta\varpi^2+\zeta^3+2\zeta}{\sqrt{\varpi^2-1}(\varpi^2-\zeta^2)^{1.5}}\frac{\partial^2\psi}{\partial\zeta^2} + \frac{\mu}{c^2}\frac{1-\zeta^2}{\sqrt{\varpi^2-1}\sqrt{\varpi^2-\zeta^2}}\frac{\partial^3\psi}{\partial\zeta^3}. \tag{23}$$

As represented in Fig. 2 at the location of the throat of the venturi, we have $\xi = 0$ [which corresponds to $\varpi = 1$ according to Eq. (3)]. Also, at the infinity ($\xi \to \infty$), we have $\varpi \to \infty$. On the other hand, because of the symmetry, the pressure drop from $\varpi \to -\infty$ to the throat is equal to the pressure drop from the throat to $\varpi \to \infty$. Therefore, the pressure drop of the flow through the plate with the gap may be calculated using the following relation:

$$\Delta P = 2\int_1^\infty \frac{\partial P}{\partial\varpi}d\varpi. \tag{24}$$

According to Eq. (23), $\partial P/\partial\varpi$ is a function of ϖ and ζ. On the other hand, in Eq. (24), the integral is only with respect to ϖ. Thus, we can substitute a specific value for ζ in Eq. (24). We set $\zeta = 0$ [which corresponds to the venturi tube axis according to Eq. (3)] in Eq. (23) and substitute the result into Eq. (24). These lead to

$$\Delta P = 2\frac{\mu}{c^2}\int_1^\infty\left(\frac{-\varpi^2\sqrt{\varpi^2-1}+\varpi^2}{\varpi^5}\frac{\partial\psi}{\partial\zeta} + \frac{1}{\varpi\sqrt{\varpi^2-1}}\frac{\partial^3\psi}{\partial\zeta^3}\right)d\varpi = 2\frac{\mu}{c^2}\left[\left(-\frac{\pi}{4}+\frac{1}{2}\right)\frac{\partial\psi}{\partial\zeta}+\frac{\pi}{2}\frac{\partial^3\psi}{\partial\zeta^3}\right]. \tag{25}$$

Now, we solve Eq. (16) with its three boundary conditions [Eq. (17) to Eq. (19)] using a numerical algorithm. Therefore, the unknown parameters of Eq. (24) are obtained as follows:

$$\left(\frac{\partial\psi}{\partial\zeta}\right)_{\zeta=0} = 0.6532q, \qquad \left(\frac{\partial^3\psi}{\partial\zeta^3}\right)_{\zeta=0} = 0.696q, \tag{26}$$

where q is the volumetric flow rate of the venturi tube. We name the gap width s. As stated previously, the gap width is $2c$ and, as a result, $c = s/2$. By substituting $c = s/2$ and Eq. (26) to Eq. (25), the pressure drop through the plate with a gap with the width s becomes

$$\Delta P = 10.2372\frac{\mu q}{s^2}, \tag{27}$$

where q and μ are volumetric flow rate and viscosity of the fluid that passes through the gap. In the topic of droplet breakup in an asymmetric T junction, one can suppose that the volume ratio of two generated droplets is equal to the ratio of the flow rate of the continuous fluid that passes through the branches [18].

C. Calculating the volume ratio, droplet length, and pressure drop

In the T junction with the valve (Fig. 1), the pressure drop of each of the branches is the sum of the pressure drop of the straight tube (calculated using the Darcy-Weisbach relation $\frac{32\mu Lq}{w^3}$) and the pressure drop of the valve. The valve is as a plate with a gap (Fig. 1). Thus, one can calculate its pressure drop using Eq. (27). On the other hand, the pressure in the outlet of each of the branches is equal to the ambient pressure. Thus, the pressure drops of the two branches (from the center of the junction to the branch outlet) are equal as follows:

$$10.2372\frac{\mu q_1}{s_1^2}+\frac{32\mu L_1 q_1}{w^3} = 10.2372\frac{\mu q_2}{s_2^2}+\frac{32\mu L_2 q_2}{w^3}. \tag{28}$$

We define three dimensionless variable as $\alpha = L/w$, $\beta = s/w$, and $\lambda = \beta_1/\beta_2$. As previously expressed, λ is the valve ratio and has an important role in the T junction with valve performance. By simplifying Eq. (28), one can calculate the volume ratio as $\beta_2 = 0$

$$\tau = \frac{V_1}{V_2} = \frac{q_1}{q_2} = \frac{\lambda^2+3.1259\alpha\beta_1^2}{1+3.1259\alpha\beta_1^2}, \tag{29}$$

where V_1 and V_2 are the volume of droplets in branches 1 and 2, respectively. We can check Eq. (29) in some particular situations. If valve 1 (valve 2) is closed, namely, $\beta_1 = 0$ ($\beta = 0$), and valve 2 (valve 1) is open (the opening degree is not important), then the droplet does not break and goes to branch 2 (branch 1) and the volume ratio becomes zero (infinity). Equation (29) gives exactly the same results, namely, for $\beta_1 = 0$ ($\beta_2 = 0$) the volume ratio becomes zero (infinity). If the opening degrees of two valves are equal, we have a symmetric T junction and the volume ratio is 1. Equation (29) gives exactly the same result, namely, for $\beta_1 = \beta_2$, the volume ratio becomes 1.

We assume the front surfaces of the droplets are circular during the breakup process (Fig. 1). Our numerical results and previous studies [45] confirm this assumption. According to the asymmetry of the breakup process, the curvature radii of the two parts of the droplets that are in the branches are different. Now we investigate analytically the droplet deformation process during the breakup. We consider the moment that the droplet is in the state of Fig. 7(c) as the initial time ($t = 0$). After time t, the volume of the continuous fluid that enters branch 1 is equal to the volume of the OAE section in Fig. 1 and is equal to the following relation:

$$V_{\mathrm{OAE}} = \tfrac{1}{2}r_1^2\left(\theta_1 - \tfrac{1}{2}\sin 2\theta_1\right). \tag{30}$$

On the other hand, the volume of the continuous fluid that enters branch 1 after time t is equal to $q_1 t$ and, according to Eq. (29), is equal to $\frac{\tau}{1+\tau}qt$ (q_1 is the volumetric flow rate of the continuous fluid of branch 1). By substituting this relation to Eq. (30), we obtain

$$\frac{\tau}{1+\tau}q = \frac{1}{2}r_1^2\left(\theta_1 - \frac{1}{2}\sin 2\theta_1\right). \tag{31}$$

Through a similar procedure for branch 2, one has

$$\frac{1}{1+\tau}q = \frac{1}{2}r_2^2\left(\theta_2 - \frac{1}{2}\sin 2\theta_2\right). \tag{32}$$

According to Eq. (29), $\tau = V_1/V_2$. Thus, $V_1 = \frac{\tau}{1+\tau}V_{\text{total}}$ where V_{total} is the volume of the whole droplet that is equal to $(L_{\text{initial}} - w)w + \frac{\pi w^2}{4}$ with L_{initial} as the droplet length before arriving to the center of the junction. It is assumed that the droplet front is circular. It is clear that the droplet front radius is half the channel width $(w/2)$. Thus, we get

$$V_1 = \frac{\tau}{1+\tau}\left[(L_{\text{initial}} - w)\,w + \pi\frac{w^2}{4}\right]. \tag{33}$$

At the end of the breakup process, the droplet breaks at point E (see Fig. 1) because the droplet has its minimum thickness in this point. Therefore, the volume of the droplet that enters branch 1 after the breakup (V_1) is

$$V_1 = \tfrac{1}{2}r_1^2\sin\theta_1\cos\theta_1 + w\,r_1\sin\theta_1 - \tfrac{1}{2}\theta_1 r_1^2 + z_1 w + \tfrac{1}{8}\pi w^2. \tag{34}$$

By substituting Eq. (33) to Eq. (34), we have

$$z_1 = \frac{1}{2w}r_1^2\left(\theta_1 - \frac{1}{2}\sin 2\theta_1\right) - r_1\sin\theta_1 + \frac{\tau}{1+\tau}\left[(L_{\text{initial}} - w) + \pi\frac{w}{4}\right] - \frac{1}{8}\pi w. \tag{35}$$

If we substitute the value of $(\theta_1 - \frac{1}{2}\sin 2\theta_1)$ from Eq. (31) to Eq. (35) and also use the relation $q/w = U_{\text{in}}$, after some simplifications we obtain

$$z_1 = \frac{\tau}{1+\tau}\left[U_{\text{in}}t + L_{\text{initial}} + \left(\frac{\pi}{4} - 1\right)w\right] - r_1\sin\theta_1 - \frac{\pi w}{8}. \tag{36}$$

Similarly for branch 2, we can achieve the following relation:

$$z_2 = \frac{1}{1+\tau}\left[U_{\text{in}}t + L_{\text{initial}} + \left(\frac{\pi}{4} - 1\right)w\right] - r_2\sin\theta_2 - \frac{\pi w}{8}. \tag{37}$$

Now we want to calculate the droplet length during the deformation in the center of the junction. The length of the small droplet (L_1) and the length of the large droplet (L_2) are depicted in Fig. 1. The droplet length in branch 1 is

$$L_1 = r_1\sin\theta_1 + z_1 + \frac{w}{2}. \tag{38}$$

By substituting $r_1\sin\theta_1 + z_1$ from Eq. (36) to Eq. (38), one obtains

$$\frac{L_1}{w} = \frac{\tau}{1+\tau}\left[\frac{U_{\text{in}}t}{w} + \frac{L_{\text{initial}}}{w} + \frac{\pi}{4} - 1\right] + \frac{1}{2} - \frac{\pi}{8}. \tag{39}$$

Similarly, for the length of the droplet that enters branch 2, we have

$$\frac{L_2}{w} = \frac{1}{1+\tau}\left[\frac{U_{\text{in}}t}{w} + \frac{L_{\text{initial}}}{w} + \frac{\pi}{4} - 1\right] + \frac{1}{2} - \frac{\pi}{8}. \tag{40}$$

Also we define the *whole droplet length* as $L_{\text{whole}} = \frac{L_1+L_2}{2}$.

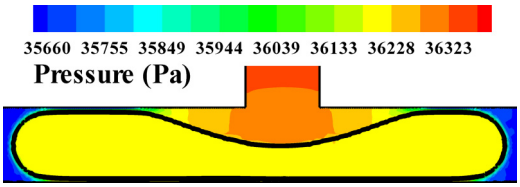

FIG. 4. (Color online) Pressure distribution during the breakup process. As is evident, the pressure inside the droplet is almost uniform.

When the droplet deforms in the center of the junction, the pressure drop of the system is the sum of these cases: (1) pressure drop in the inlet channel (from the inlet of the system to center of junction) that can be calculated using the Darcy-Weisbach relation; (2) pressure difference between the inside and the outside of the droplet in the center of the junction, that is, the difference of the fluid pressure between slightly above and slightly below point E (see Fig. 1) which is equal to σ/r where r is the curvature radius of the interface; (3) With a good approximation, the fluid pressure inside the droplet is uniform. Both our numerical results (Fig. 4) and previous studies [45] confirm this point. Therefore, there is no pressure drop inside the droplet; (4) pressure difference inside and outside of the droplet in the droplet tip location, namely, the difference of the fluid pressure between slightly left and slightly right of point F (see Fig. 1) which is equal to $2\sigma/w$; (5) pressure drop of fluid in the straight tube after droplet tip (point F to the end of the branch in Fig. 1) that can be calculated using the Darcy-Weisbach relation. The length of the tube in this case is equal to the difference of the branch length (L in Fig. 1) and the droplet length during deformation [Eq. (39)]; (6) pressure drop due to the valve that calculates using Eq. (29) $(10.2372\mu q/s^2)$. The location of the valve does not affect the pressure drop because it is far enough from the droplet tip and the branch outlet.

Our numerical results and other investigations [45] confirm that the pressure drop of case (2) is negligible in comparison with that of case (4). Therefore, the pressure drop of the system may be calculated by the following relation:

$$\Delta P = \frac{32\mu U_{\text{in}}L_{\text{in}}}{w^2} + \frac{32\mu\tau U_{\text{in}}(L - L_1)}{w^2(1+\tau)} + \frac{2\sigma}{w} + \frac{10.2372\mu\tau U_{\text{in}}}{s_1^2(1+\tau)}, \tag{41}$$

where μ is the continuous fluid viscosity, U_{in} is the inlet velocity of the system, L_{in} is the length of the inlet channel, L_1 is the droplet length in branch 1 that is calculated from Eq. (39), L is the length of the branch (Fig. 1), τ is the volume ratio that is derived using Eq. (29), and s_1 is the opening degree of the valve of branch 1.

IV. NUMERICAL SIMULATION

For simulating the two phase flow, a VOF algorithm is employed. Also for simulation of the system, other numerical methods such as the lattice Boltzmann method can be employed [51–53]. The flow is assumed to be incompressible

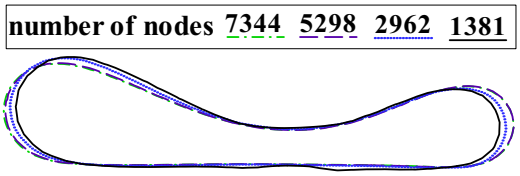

FIG. 5. (Color online) Grid independency results.

and the governing equations are Navier-Stokes and continuity as follows:

$$\frac{\partial u_i}{\partial x_i} = 0, \tag{42}$$

$$\rho\left(\frac{\partial u_i}{\partial t} + u_j\frac{\partial u_i}{\partial x_j}\right) = -\frac{\partial P}{\partial x_i} + F_i + \mu\frac{\partial^2 u_i}{\partial x_j^2}, \tag{43}$$

where u_i is the velocity vector and ρ and μ are density and viscosity of the fluid, respectively, and are calculated as follows:

$$\rho = \rho_c\phi + \rho_d\,(1-\phi)\,, \tag{44}$$

$$\mu = \mu_c\phi + \mu_d\,(1-\phi)\,, \tag{45}$$

where the subscripts c and d refer to the continuous (that carries the droplets) and the dispersed (droplet) phases and ϕ is the volume fraction of the continuous phase in each of the computational cells and we have $0 \leqslant \phi \leqslant 1$. The exact location of the interface is where we have $\phi = 0.5$, which is calculated using a piecewise linear interface reconstruction method. ϕ is calculated using the following relation:

$$\frac{\partial \phi}{\partial t} + u_i\frac{\partial \phi}{\partial x_i} = 0. \tag{46}$$

The momentum equation is discretized using a second-order upwind method. Pressure velocity coupling is performed using a SIMPLEC algorithm. The convergence criterion is the residuals that are calculated using the following equation to be less than 0.0007:

$$R_X = \frac{\sum_{P=1}^{N}\left|\sum_{nb} a_{nb}X_{nb} + \Phi - a_P X_P\right|}{\sum_{P=1}^{N} a_P X_P}, \tag{47}$$

where X is a general variable in the cell P, N is the number of all computational cells, a_P is the center coefficient (cell P), a_{nb} is the coefficient of the neighboring cells of the cell P, and Φ is the constant part of the source term ($S = S_c + S_P X$) and of the boundary conditions.

Grid independency is performed using the simulation of the droplet breakup problem. At the moment that the droplet deforms in the center of junction, the droplet profile is compared in various grid sizes. The results of the comparison are shown in Fig. 5. As seen in Fig. 5, for the grids with more than 5298 nodes, the results are grid independent.

In a symmetric T junction, for the lengths of the droplet before arriving at the center of the junction that are smaller than a specific value (critical length), the droplet does not break. Leshansky and Pismen [45] have derived a relation for droplet critical length in a symmetric T junction as a function of the capillary number ($l/w = 1.3\ \mathrm{Ca}^{-0.21}$). For checking the accuracy of our numerical results, their problem [45] was simulated and the results were compared with their analytical relation and very good agreement was observed [41]. Also, Bretherton [46] has reported the droplet velocity for a moving droplet through a circular tube and derived as $U = \bar{U}[1 + 1.29(\mu_c U/\sigma)^{2/3}]$ with U as the droplet velocity and σ, μ_c, and $\bar{U}$ as the surface tension between two fluids, viscosity, and average velocity of continuous fluid, respectively. For verifying the accuracy of our simulation, we also compared our numerical results with the relation of Bretherton and very good agreement was achieved [41].

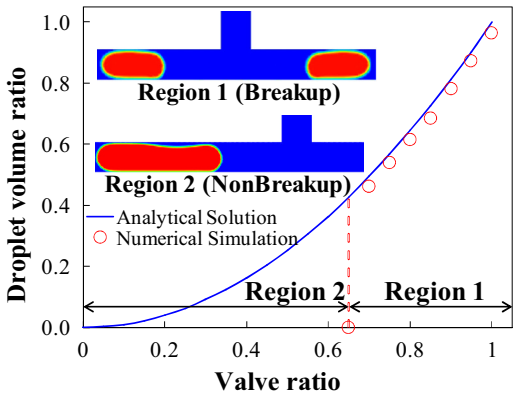

FIG. 6. (Color online) Droplet volume ratio as a function of the valve ratio. Analytical results [Eq. (29)] have very good agreement with the numerical results. In the valve ratios smaller than 0.65, the droplet does not break. The numerical simulation is done for $\mathrm{Ca} = 0.01$ and the initial length of the droplet is equal to $6w$.

V. RESULTS AND DISCUSSION

In this section, the results of the analytical analysis are presented and compared with the numerical solution. Operating conditions have important effects on the droplet performance [54]. Thus, we investigate the effect of important parameters such as valve ratio, inlet velocity of the system, and initial length of the droplet on the breakup performance of the droplet in the T junction with the valve.

Figure 6 compares the analytical [Eq. (29)] and numerical results for the volume ratio as a function of the valve ratio and very good agreement is evident. The numerical results show that there are two regions in Fig. 6. Region 1 is the breakup region and includes the valve ratios larger than 0.65 and region 2 is the nonbreakup region and includes the valve ratios smaller than 0.65. As seen, the analytical theory cannot predict the boundary of the breakup and nonbreakup regions. For prediction of this boundary, a more sophisticated approach is required to analyze the surface tension and inertial forces when the droplet is deforming in the center of the junction. An example of the droplet motion in regions 1 and 2 is depicted in Fig. 6. With respect to Fig. 6, the volume ratio increases by increasing the valve ratio.

A sample of the droplet breakup process is illustrated in Fig. 7. As can be seen in Fig. 7(f), after droplet breakup, two large vortexes are generated in the continuous fluid in the center of the junction. Vortex generation is the result of the fast motion of the fronts of the new droplets after breakup.

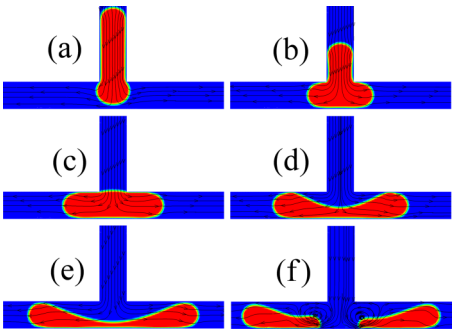

FIG. 7. (Color online) A sample of the long-droplet breakup process. The streamlines are depicted in the figure.

Figure 8 illustrates the analytical [Eqs. (39) and (40)] and numerical results of the droplet length as a function of time at the valve ratios 0.7, 0.8, and 0.9 and very good agreement exists. The numerical results of Fig. 8 are related to a T junction with channel width $w = 20 \times 10^{-6}$m, droplet initial length $6w$, and inlet velocity of the system 0.04 m/s. As is evident in Fig. 8, the droplet length increases linearly with time. The slope of the droplet length curves represents the continuous fluid velocity of branches 1 and 2 [Eqs. (39) and (40)]. On the other hand, the continuous fluid velocity of the branches that were calculated using the analytical and numerical results have a small difference. For this reason, a small difference exists between the analytical and numerical results in some cases of Fig. 8. As already stated, for the valve ratios smaller than 0.65, the droplet does not break and is situated in the nonbreakup region (Fig. 6). Therefore, for the case $\lambda = 0.7$, the droplet behavior is very close to the nonbreakup mode. In this case, the part of the droplet that exists in branch 1 tends to return to branch 2 due to the high continuous fluid velocity of branch 2 and the surface tension effects. Therefore, during the breakup process, the growth rate of the droplet length in branch 1 reduces. Because of this reason, for $\lambda = 0.7$ of Fig. 8, the slope of the L_1/w curve reduces after a while.

Also, by calculating the different valve ratio diagrams, one can conclude that by decreasing (increasing) the valve ratio, the droplet length of branch 1 decreases (increases) and the droplet length of branch 2 increases (decreases) because a smaller (larger) droplet enters branch 1. Also the whole length of the droplet (L_{whole}) does not depend on the valve ratio. The droplet length defines until breakup moment. After breakup of the droplet, we do not need the droplet length parameter because the initial droplet is broken and the process is finished and we should exit two generated droplets from the system.

Figure 9 illustrates the analytical [Eqs. (39) and (40)] and numerical results of the droplet length as a function of time in various initial droplet lengths (L_{initial}) and inlet velocities of the system (U_{in}). For a specific droplet initial length, by increasing (decreasing) the inlet velocity, the increase rate of the L_1, L_2, and L_{whole} increase (decrease) because the speed of the droplets in channels 1 and 2 increases (decreases). Also, by increase (decrease) of the droplet initial length, L_1, L_2, and L_{whole} increase (decrease). The results illustrate that during the time a constant difference exists between two curves with different droplet initial lengths. Therefore, to decrease the droplet length and reduce the pressure drop and system manufacturing costs,

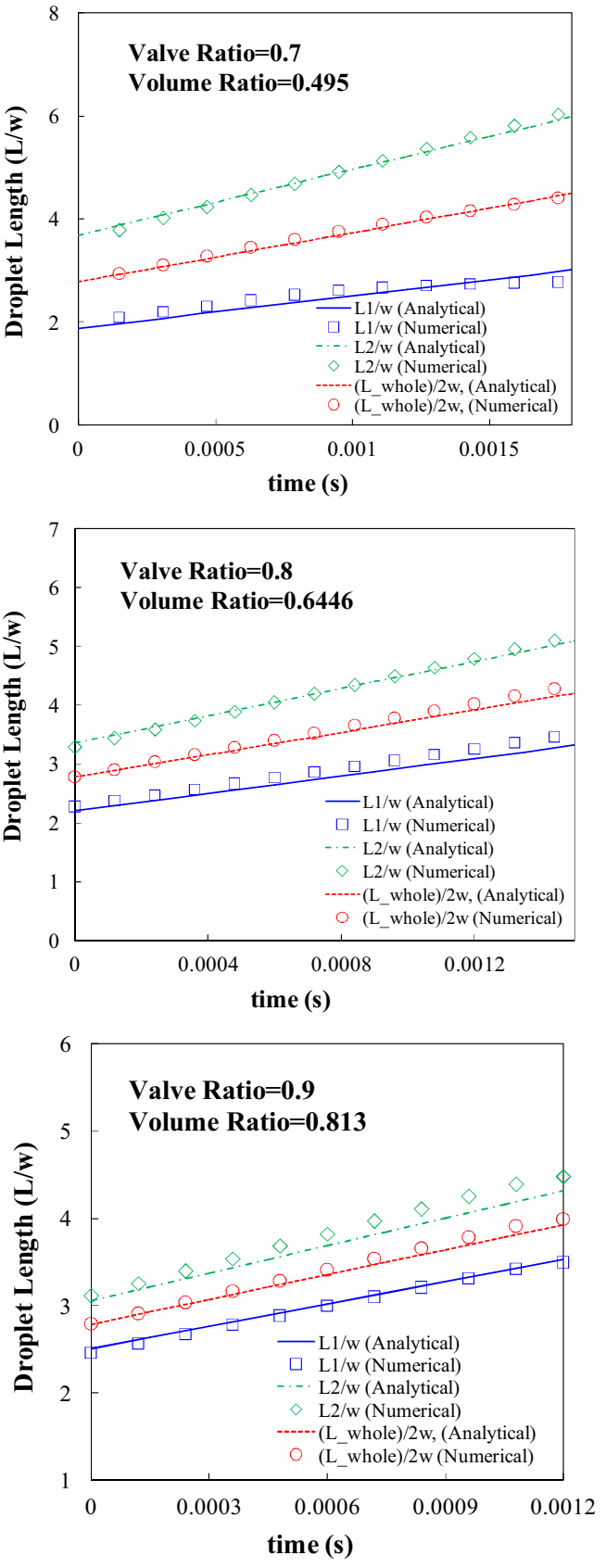

FIG. 8. (Color online) Analytical [Eqs. (39) and (40)] and numerical results of the droplet length as a function of time at valve ratios 0.7, 0.8, and 0.9. The droplet length is scaled with the channel width (w).

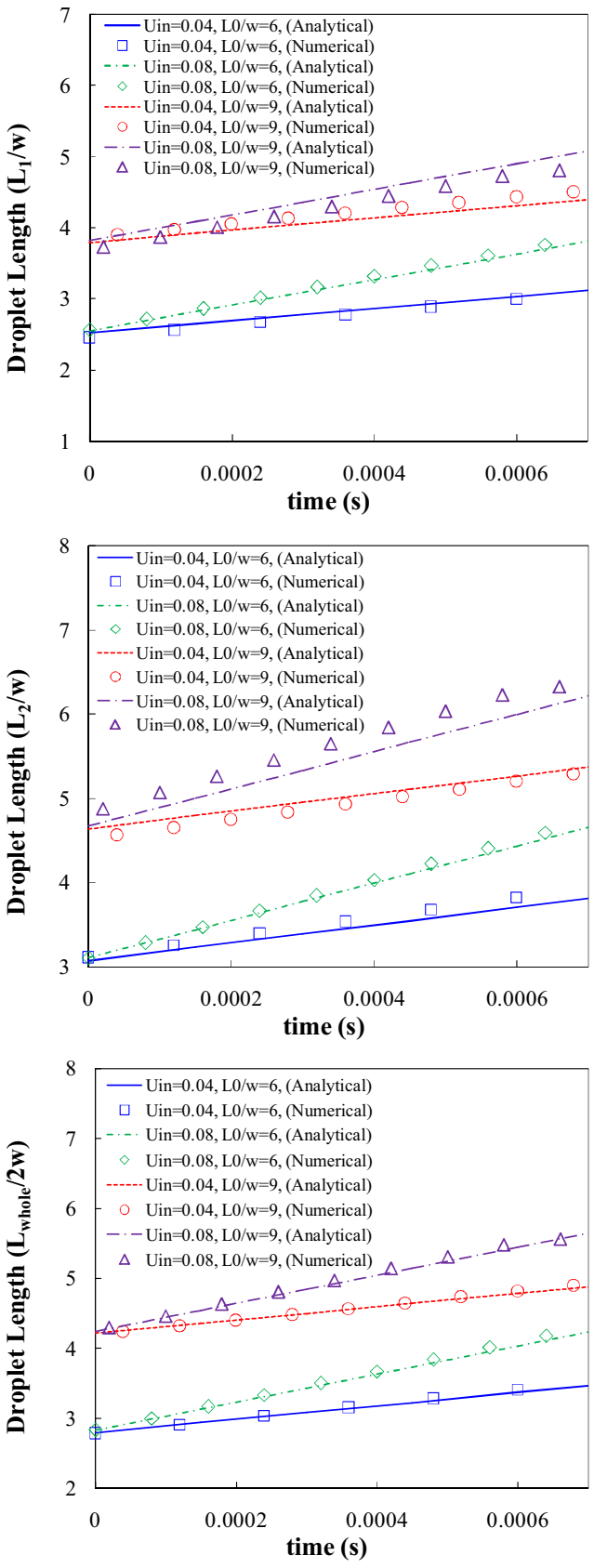

FIG. 9. (Color online) Analytical [Eqs. (39) and (40)] and numerical results of the droplet length as a function of time at inlet velocities 0.04 and 0.08 and initial lengths 6 and 9. The droplet length has been scaled with the channel width (w).

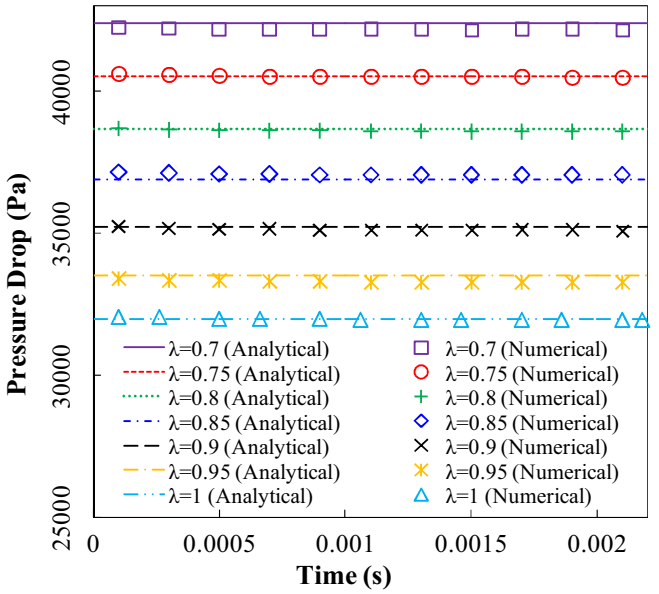

FIG. 10. (Color online) Analytical relation [Eq. (41)] and numerical results of the pressure drop of the T junction with valve. The pressure drop is calculated as the pressure difference between the inlet of the system and one of the two outlets. As is seen, by increasing the symmetry of the geometry, the pressure drop reduces and the minimum pressure drop relates to the symmetric T junction.

the droplet initial length and inlet velocity of the system should be reduced as much as possible.

Figure 10 depicts the analytical [Eq. (41)] and numerical results of the system pressure drop as a function of time in the valve ratios 0.7, 0.75, 0.8, 0.85, 0.9, 0.95. and 1.0. The

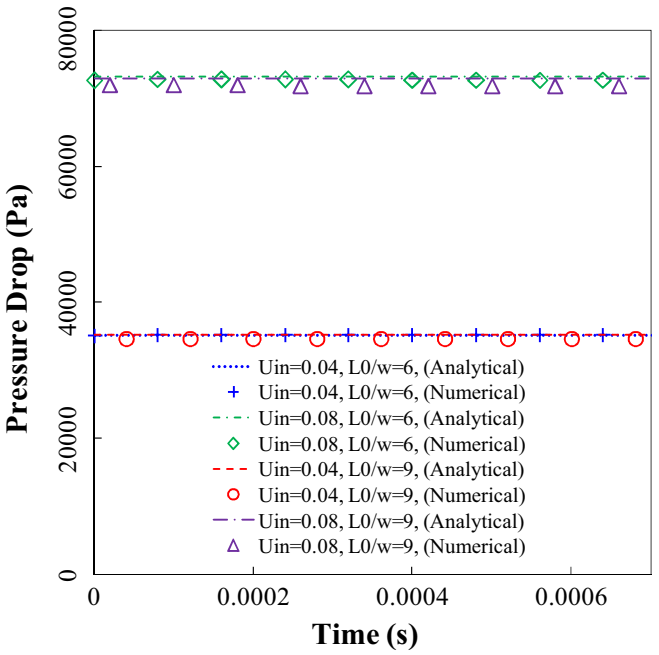

FIG. 11. (Color online) Analytical [Eq. (41)] and numerical results of the system pressure drop in various droplet initial lengths ($6w$ and $9w$) and system inlet velocities (0.04 m/s and 0.08 m/s). As can be seen, the pressure drop in all of the cases does not change by an increase of the time.

pressure drop is calculated from the system inlet to the outlet of the branches. There is a very good agreement between the analytical and the numerical results. The numerical results are related to a T junction with the same characteristics of the T junction that is mentioned in Fig. 8 with $L_{\text{in}} = 9w$, $L = 16w$, $\mu = 0.00125$ Pa s, and $\sigma = 0.005$ N/m. Figure 10 illustrates that the pressure drop has a very low dependence on the time. Also, by increasing the valve ratio and tending the system to a symmetric T junction, the pressure drop reduces. Therefore, to reduce the pressure drop, the valve ratio should be increased so that the system becomes more symmetric.

Figure 11 depicts the analytical [Eq. (41)] and numerical solution of the pressure drop as a function of the time in various droplet initial lengths and system inlet velocities. As is evident in Fig. 11, the system pressure drop has a large dependency on the system inlet velocity and by an increase (decrease) of the inlet velocity, the pressure drop increases (decreases). This is due to the fact that the system inlet velocity has a significant effect on the pressure drop of the valves and tubes. Also, the droplet initial length has a negligible effect on the pressure drop because the fluid pressure inside the droplet is uniform, as already stated. Therefore, to reduce the system pressure drop, the system inlet velocity should be reduced as much as possible.

VI. CONCLUSION

In this paper, we investigated T junctions with valves for producing unequal-sized droplets. We developed a comprehensive analytical theory for the system. Also the geometry was simulated using a VOF algorithm and a comparison was performed between numerical and analytical results and very good agreement was observed. The accuracy of numerical results was confirmed by comparing the results with two analytical benchmarks. We derived accurate analytical relations for calculating the droplet volume ratio, droplet length (L_1, L_2, and L_{whole}), and pressure drop of the system. We observed that if the valve ratio becomes less than a specific value (0.65), the system enters the nonbreakup region. Both the analytical theory and the numerical results showed that by decreasing (increasing) the valve ratio, the droplet length of branch 1 decreases (increases) and the droplet length of branch 2 increases (decreases), and the whole length of the droplet remains constant. The results showed that the system pressure drop does not depend on the time and decreases by increasing the valve ratio, namely, leading the geometry to a symmetric T junction. Both the analytical theory and the numerical results showed that the droplet length in branches 1 and 2 and the whole droplet length increase linearly with time. Also, it was shown that the growth rate of L_2 is greater than that of L_1 and, by decreasing (increasing) the valve ratio, the growth rate of L_1 decreases (increases) and the growth rate of L_2 increases (decreases). As already stated, although the results of this study belong to 2D systems, based on previous studies [41,55], similar qualitative results can be expected for 3D systems.

[1] X. Sun, K. Tang, R. D. Smith, and R. T. Kelly, Microfluid. Nanofluid. **15**, 117 (2013).
[2] S. Zhao, W. Wang, M. Zhang, T. Shao, Y. Jin, and Y. Cheng, Chem. Eng. J. **207**, 267 (2012).
[3] D. A. Sessoms, M. Belloul, W. Engl, M. Roche, L. Courbin, and P. Panizza, Phys. Rev. E **80**, 016317 (2009).
[4] M. De Menech, Phys. Rev. E **73**, 031505 (2006).
[5] D. A. Hoang, L. M. Portela, C. R. Kleijn, M. T. Kreutzer, and V. V. Steijn, J. Fluid Mech. **717**, R4 (2013).
[6] K. Golemanov, S. Tcholakova, N. D. Denkov, K. P. Anantha-padmanabhan, and A. Lips, Phys. Rev. E **78**, 051405 (2008).
[7] L. Ménétrier-Deremble and P. Tabeling, Phys. Rev. E **74**, 035303 (2006).
[8] K. L. Pan, P. C. Chou, and Y. J. Tseng, Phys. Rev. E **80**, 036301 (2009).
[9] B. Xu, N. T. Nguyen, and T. N. Wong, Biomicrofluidics **6**, 012811 (2012).
[10] O. Carrier, D. Funfschilling, and H. Z. Li, Phys. Rev. E **89**, 013003 (2014).
[11] P. Laval, N. Lisai, J. B. Salmon, and M. Joanicot, Lab Chip **7**, 829 (2007).
[12] H. Liu and Y. Zhang, J. Appl. Phys. **106**, 034906 (2009).
[13] G. F. Christopher, N. N. Noharuddin, J. A. Taylor, and S. L. Anna, Phys. Rev. E **78**, 036317 (2008).
[14] J. Tice, H. Song, A. Lyon, and R. Ismagilov, Langmuir **19**, 9127 (2003).
[15] A. Bedram and A. Moosavi, J. Appl. Fluid Mech. **6**, 81 (2013).
[16] T. Fu, Y. Ma, D. Funfschilling, and H. Z. Li, Chem. Eng. Sci. **66**, 4184 (2011).
[17] S. Afkhami, A. M. Leshansky, and Y. Renardy, Phys. Fluids **23**, 022002 (2011).
[18] D. R. Link, S. L. Anna, D. A. Weitz, and H. A. Stone, Phys. Rev. Lett. **92**, 054503 (2004).
[19] A. Bedram and A. Moosavi, Eur. Phys. J. E **34**, 78 (2011).
[20] B. R. Sehgal, R. R. Nourgaliev, and T. N. Dinh, Prog. Nucl. Energy **34**, 471 (1999).
[21] J. H. Choi, S. K. Lee, J. M. Lim, S. M. Yang, and G. R. Yi, Lab Chip **10**, 456 (2010).
[22] T. H. Ting, Y. F. Yap, N. T. Nguyen, T. N. Wong, J. C. K. Chai, and L. Yobas, Appl. Phys. Lett. **89**, 234101 (2006).
[23] S. Galinat, O. Masbernat, P. Guiraud, C. Dalmazzone, and C. Noïk, Chem. Eng. Sci. **60**, 6511 (2005).
[24] R. Skartlien, E. Sollum, and H. Schumann, J. Chem. Phys. **139**, 174901 (2013).
[25] F. Ravelet, C. Colin, and F. Risso, Phys. Fluids **23**, 103301 (2011).
[26] Q. Li, Z. Chai, B. Shi, and H. Liang, Phys. Rev. E **90**, 043015 (2014).
[27] T. Cubaud, Phys. Rev. E **80**, 026307 (2009).
[28] F. Abbassi, B. Mosto, and M. A. Huneault, Rheolog. Acta **51**, 111 (2012).
[29] A. Vananroye, P. V. Puyvelde, and P. Moldenaers, Langmuir **22**, 3972 (2006).
[30] J. G. Hagedorn, N. S. Martys, and J. F. Douglas, Phys. Rev. E **69**, 056312 (2004).
[31] Y. Chen, X. Liu, and M. Shi, Appl. Phys. Lett. **102**, 051609 (2013).

[32] G. F. Christopher, J. Bergstein, N. B. End, M. Poon, C. Nguyen and S. L. Anna, Lab Chip **9**, 1102 (2009).
[33] J. Nie and R. T. Kennedy, Anal. Chem. **82**, 7852 (2010).
[34] W. Engl, M. Roche, A. Colin, P. Panizza, and A. Ajdari, Phys. Rev. Lett. **95**, 208304 (2005).
[35] I. Lee, Y. Yoo, Z. Cheng, and H. K. Jeong, Adv. Funct. Mater. **18**, 4014 (2008).
[36] W. Yining, F. Taotao, C. Zhu, Y. Lu, Y. Ma, and H. Z. Li, Microfluid. Nanofluid. **13**, 723 (2012).
[37] V. Cristini, J. Bławzdziewicz, and M. Loewenberg, Phys. Fluids **10**, 1781 (1998).
[38] D. D. Joseph, J. Belanger, and G. S. Beavers, Int. J. Multiphase Flow **25**, 1263 (1999).
[39] A. J. Griggs, A. Z. Zinchenko, and R. H. Davis, Int. J. Multiphase Flow **34**, 408 (2008).
[40] S. S. Sazhin, W. A. Abdelghaffar, E. M. Sazhina, and M. R. Heikal, Int. J. Thermal Sci. **44**, 610 (2005).
[41] A. Bedram, A. E. Darabi, A. Moosavi, and S. Kazemzade, ASME J. Fluids Eng. **137**, 031202 (2014).
[42] J. D. Crounse, K. A. McKinney, A. J. Kwan, and P. O. Wennberg, Anal. Chem. **78**, 6726 (2006).
[43] N. Wongprasert and M. D. Symans, ASCE J. Struc. Eng. **131**, 867 (2005).
[44] S. S. Parmar and S. W. Benson, J. Phys. Chem. **92**, 2652 (1988).
[45] A. M. Leshansky and L. M. Pismen, Phys. Fluids **21**, 023303 (2009).
[46] F. P. Bretherton, J. Fluid Mech. **166**, 10 (1961).
[47] V. V. Steijn, C. R. Kleijn, and M. T. Kreutzer, Lab Chip **10**, 2513 (2010).
[48] W. Gibbs and E. B. Wilson, *Vector Analysis* (Yale University Press/Dover, New York, 1960),
[49] M.R. Spiegel, L. Lipschutz, and D. Spellman, *Vector Analysis, 2nd* ed. (McGraw Hill, New York, 2009).
[50] R. W. Fox, A. T. McDonald, and P. J. Prichard, *Introduction to Fluid Mechanics*, 6th ed. (Wiley, New York, 2003).
[51] Z. Guo, H. Han, B. Shi, and C. Zheng, Phys. Rev. E **79**, 046708 (2009).
[52] Q. Li, Y. L. He, G. H. Tang, and W. Q. Tao, Phys. Rev. E **81**, 056707 (2010).
[53] S. Srivastava, P. Perlekar, Jan M. H. ten Thije Boonkkamp, N. Verma, and F. Toschi, Phys. Rev. E **88**, 013309 (2013).
[54] M. L. J. Steegmans, C. Schroen, and R. M. Boom, Chem. Eng. Sci. **64**, 3042 (2009)
[55] M. C. Jullien, M. J. T. M. Ching, C. Cohen, L. Menetrier, and P. Tabeling, Phys. Fluids **21**, 072001 (2009).